J. Fluid Mech. (1976), *vol.* 78, *part* 2, *pp.* 289–315
Printed in Great Britain

Turbulent flow in a rectangular duct

By A. MELLING AND J. H. WHITELAW
Department of Mechanical Engineering, Imperial College, London

(Received 13 January 1976 and in revised form 14 June 1976)

A detailed experimental study of developing turbulent flow in a rectangular duct was made using a laser-Doppler anemometer. The purposes of the work were to obtain data of value to fluid mechanicists, particularly those interested in the development and testing of mathematical turbulence models, and to evaluate the performance of the anemometer. For the first purpose, contours of axial mean velocity and turbulence intensity were measured in the developing flow, and all three mean velocity components and five of the six Reynolds stresses were obtained in the nearly fully developed flow.

The symmetry of the present flow appears to be better than that of previous measurements and the range of measurements is more extensive. In addition, the laser-Doppler anemometer has the potential advantage, particularly in the measurement of secondary velocities, of avoiding probe interference.

1. Introduction

Many turbulent flows in engineering practice occur in ducts of non-circular cross-section; examples include heat exchangers, nuclear-reactor channels, air-conditioning systems and rotary machinery. A three-dimensional mean motion is found in all these configurations, even in fully developed flow; the resulting secondary velocity components in the cross-section of the duct may be only 1 % of the axial velocity, but exert a strong influence on both overall and local properties of the flow. Calculations of pressure drop and heat transfer, for example, should take account of the secondary motions although empirical equations for these quantities can be related to correlations in turbulent pipe flow (in which secondary flows do not exist) through the concept of a hydraulic diameter (e.g. Hartnett, Koh & McComas 1962). Mathematical models of the turbulence structure have been developed for predicting these flows, e.g. Launder & Ying (1973), Launder, Reece & Rodi (1975) and Naot, Shavit & Wolfshtein (1974); but these models must be compared with detailed data in order to verify them.

The simplest geometry in which secondary flows arise is a straight duct of square or rectangular cross-section. where they were first observed by Nikuradse (1926). He noted that contours of axial mean velocity (isovels) bulged outwards near the corners as a result of secondary motion from the centre of the duct towards the corners. Quantification of these secondary flows was not reported until Hoagland (1960) devised a hot-wire technique, which was subsequently

employed, with improved accuracy, by Brundrett & Baines (1964), Gessner (1964), Gessner & Jones (1965) and Launder & Ying (1972). Other features of these flows such as mean velocity profiles, the pressure drop and wall shear stress distributions have been measured by Leutheusser (1963), Ahmed & Brundrett (1971) and Thomas & Easter (1972). The most complete description of turbulent flow in square ducts was, however, provided by Brundrett & Baines, who measured the six Reynolds-stress components as well as the three mean velocity components. From an analysis of the transport equation for the mean axial vorticity they deduced that secondary velocities were generated by gradients of Reynolds stresses in the plane of the duct cross-section, and their data showed that the main contribution to the generation term arose from the normal stress gradients. In spite of the more recent analyses by Perkins (1970) and Gessner (1973), the work of Brundrett & Baines remains the most fruitful basis for predicting secondary flow.

These previous investigations, however, do not allow quantitative evaluation of calculation methods and the turbulence assumptions on which they are based with sufficient precision, although they do make important contributions towards it. Therefore the experiments reported in this paper were made with the aim of facilitating the assessment of turbulence models. In contrast to previous investigations, other than the preliminary work of Melling & Whitelaw (1973), the present measurements were obtained with a laser-Doppler anemometer. This allowed the measurement of the three components of mean velocity and the corresponding Reynolds stresses without the possible consequences of flow interference associated with Hoagland's hot-wire technique; it also permitted measurements to be made in the developing flow.

The next section describes the flow configuration and the laser-Doppler anemometer instrumentation. The results are presented in §3 and discussed in §4; these two sections consider the axial development of the mean velocity and streamwise turbulence intensity, and the contours of transverse turbulence intensity, Reynolds shear stress, kinetic energy and secondary mean velocity in the nearly fully developed flow. Brief conclusions are provided in §5.

2. Flow configuration and instrumentation

Flow configuration

The flow configuration used for this work was a straight duct of rectangular cross-section constructed from 9 mm thick Perspex. Water was chosen as the working fluid because it allowed almost continuous Doppler signals from the anemometer to be processed with a frequency-tracking demodulator without the addition of particles. The duct was 1·8 m long and had a cross-section 40 mm wide by 41 mm deep; the variation in these dimensions along the duct was at most $\pm 0{\cdot}2$ mm in the depth and $\pm 0{\cdot}1$ mm in the width, i.e. the maximum deviation from the average cross-sectional area was $\pm 0{\cdot}7\,\%$.

The water was pumped from a sump tank to a constant-head tank from which it flowed by gravity into a large plenum chamber, through the test section and into a discharge tank (which ensured that the test section remained full)

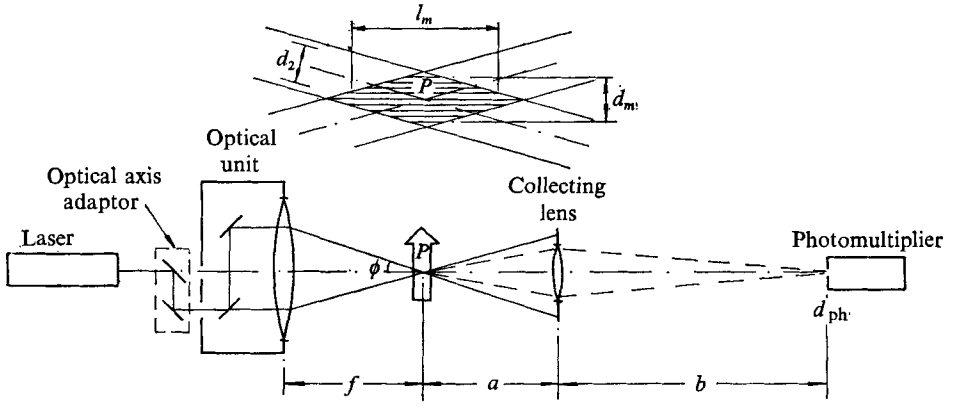

FIGURE 1. Optical arrangement for anemometer.

before finally overflowing into the sump. The system was normally operated at a flow rate of 1·50 kg/s, corresponding to a bulk velocity U_b in the test section of 0·915 m/s and a Reynolds number Re of $4{\cdot}2 \times 10^4$ based on the bulk velocity and the hydraulic diameter $D_H = 4 \times$ cross-sectional area/perimeter. The flow rate was monitored with an orifice-plate flowmeter designed in accordance with B.S. 1042. Static taps were drilled in the duct to measure the axial static pressure gradient dp/dx_1.

Optical system

The optical components of the laser-Doppler anemometer were arranged in the standard forward-scatter fringe geometry (figure 1), described, for example, by Durst, Melling & Whitelaw (1976, p. 126). The beam from a 5 mW He–Ne laser was split and the resulting beams were focused at their crossing region by an 'integrated optical unit' having a lens of focal length $f = 150$ mm. Scattered light was collected into the photomultiplier through an aperture of diameter $d_{ph} = 0{\cdot}9$ mm. The values of the parameters of the optical system defined in figure 1 were $a = 122$ mm, $b = 587$ mm and $\phi = 9{\cdot}87°$. The beam waist diameter d_2 at the e^{-2} light intensity level was calculated to be 186 μm using a laser beam of diameter $D_2 = 0{\cdot}65$ mm and the formula

$$d_2 = \frac{4}{\pi}\lambda\frac{f}{D_2}, \tag{2.1}$$

where λ is the wavelength of laser light. The diameter of the scattering volume, $d_m = 187$ μm, was controlled by the light collecting system according to the equation

$$d_m = (a/b)d_{ph}, \tag{2.2}$$

and its length, $l_m = 1{\cdot}45$ mm, was controlled by the beam waist diameter and the angle of intersection of the beams in water, i.e.

$$l_m = md_2/\sin\phi, \tag{2.3}$$

where m is the refractive index of water. The number of fringes viewed by the

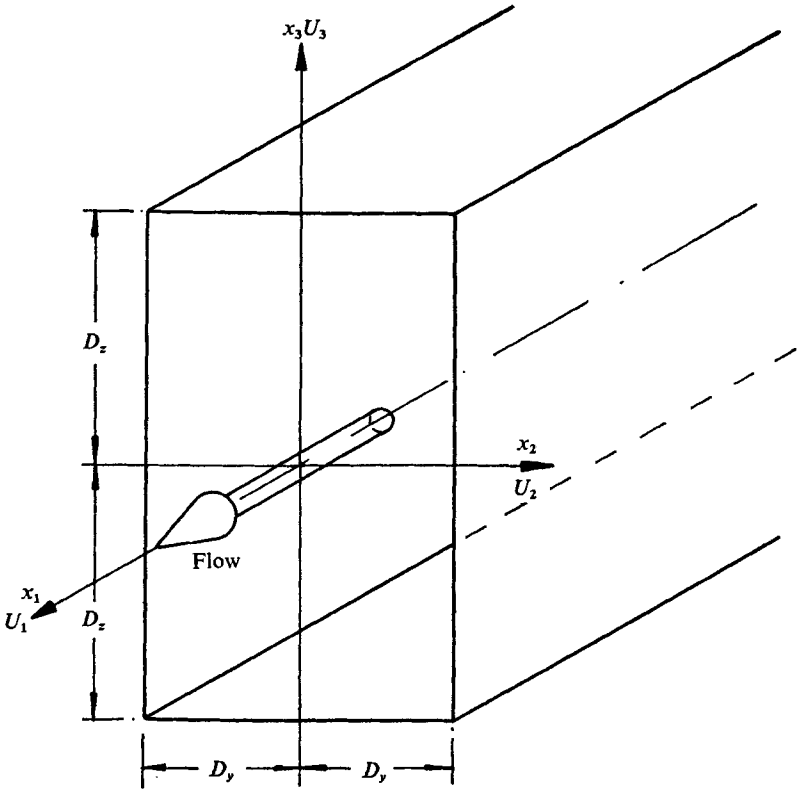

FIGURE 2. Co-ordinate system for rectangular duct (for square duct, $D_y = D_z = D$).

photomultiplier, specified by

$$N_{\mathrm{ph}} = 2d_m \sin \phi/\lambda, \tag{2.4}$$

was 100.

The optical bench was mounted to permit traversing along the three co-ordinate directions shown in figure 2. A milling machine table, calibrated to 0·001 in., provided horizontal movements in two directions; the optical bench could be moved vertically on three bolts of $\frac{1}{16}$ in. pitch. The optical system and traversing gear were mounted on a trolley to permit streamwise movement along the full length of the duct. Axial distances with respect to the duct entry were determined to within $\pm 0{\cdot}02D_H$ using a steel tape. Distances in the horizontal direction were accurate to within the smallest division of the milling-table screw, i.e. about $\pm 0{\cdot}02$ mm. In the vertical direction, accuracy was about $\pm 0{\cdot}2$ mm.

The optical system could be adjusted for measuring both streamwise and transverse components of velocity, using an optical axis adaptor to rotate the plane of the incident beams. When measuring the streamwise component, the incident beams of the anemometer were arranged to lie in the x_1, x_2 plane. Orientation of the beams in the x_2, x_3 plane would render the anemometer sensitive to the x_3 velocity component alone but, in this orientation, the fringes

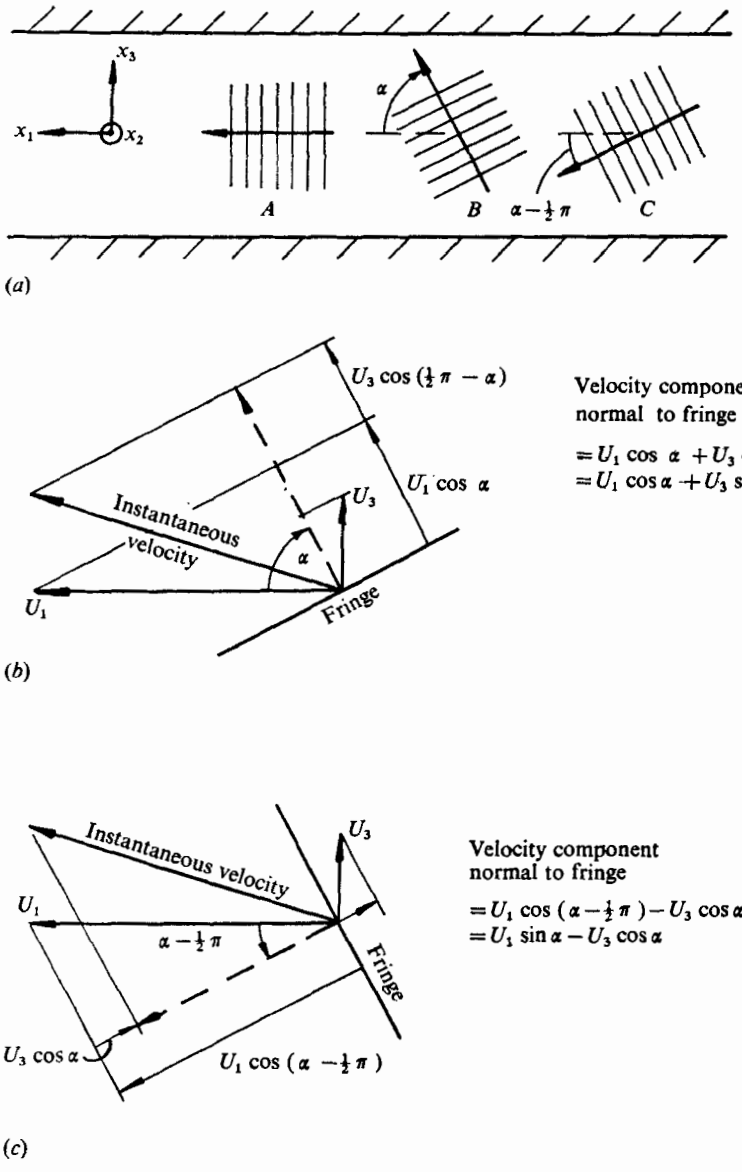

FIGURE 3. (*a*) Orientation of fringes for sensitivity to two velocity components. (*b*) Vector diagram for case *B*. (*c*) Vector diagram for case *C*.

lie nearly parallel to the instantaneous velocity vector; thus particles cross only a few fringes, giving an insufficient number of Doppler cycles for accurate processing. Moreover, the instantaneous velocity vector fluctuates above and below the x_1, x_2 plane, giving positive and negative values to the velocity component U_3, whose sign could not be distinguished. A frequency-shifting device (Durst & Zaré 1974) would have overcome these problems but an alternative procedure was to align the fringe system to be sensitive to both the U_1 and the U_3 velocity component. Measurements were made with the fringe system

orientated such that the normal to the fringes was inclined successively at angles of 0, α and $\alpha - \frac{1}{2}\pi$ to the x_1 axis, as shown schematically in figure 3(*a*). In the experiments α was taken as 45°, and the velocity components were derived from the measured Doppler frequencies using equations presented in appendix A.

To measure the velocity component U_2 the optical system was set up about a vertical axis. The parameters of this optical system were the same as for the horizontal-axis arrangement except that $a = 130$ mm and $b = 540$ mm. Thus the diameter of the control volume was 217 μm and 116 fringes were observed by the photomultiplier. Sensitivity of the vertical-axis system to the U_1 and U_2 components simultaneously was obtained by rotating the fringe system by $\pm 45°$ about the x_3 axis.

Signal-processing system

The Doppler signals were processed with a DISA 55L20 frequency tracker. The operation of frequency trackers is described, for example, by Durst *et al.* (1976, chapter 8), where it is shown that the conditions of the present experiment, i.e. moderate Doppler frequency (maximum 550 kHz), moderate turbulence intensities (up to 12 %) and a high concentration of scattering particles, were appropriate for frequency tracking. In view of the large amount of data required, the rapid data acquisition possible with a frequency tracker was a vital asset. The tracker was operated with a bandwidth (capture range) of 2 %. A narrow bandwidth improves the signal-to-noise ratio at the input to the frequency discriminator but attenuates the response of the tracker to high turbulence frequencies. According to the results of Durão & Whitelaw (1974), however, the 2 % bandwidth setting did not attenuate the response for turbulence frequencies below 1 kHz at the maximum turbulence intensities encountered in this investigation.

The output from the tracker was a voltage nominally proportional to the Doppler frequency and, hence, to the velocity component perpendicular to the fringes in the scattering volume. The output was divided between a true integrator and a true r.m.s. meter to obtain voltages proportional to the mean Doppler frequency and the r.m.s. level of fluctuations in Doppler frequency. The tracker output was also monitored on an oscilloscope so that data affected by rapid slewing of the voltage when the tracking loop unlocked from the Doppler signal ('drop-out') could be rejected.

Details of the procedure used to evaluate mean velocity components and Reynolds-stress components from the measured voltages are provided in appendix A.

3. Results

This section describes the results in the following sequence: checks on symmetry of the mean flow, mean flow properties determined by the axial pressure gradient and centre-line mean velocity, mean velocity contours (isovels) at five axial stations, axial turbulence intensity contours, transverse turbulence intensity contours, Reynolds shear stress contours, turbulence kinetic energy contours and secondary mean velocity contours.

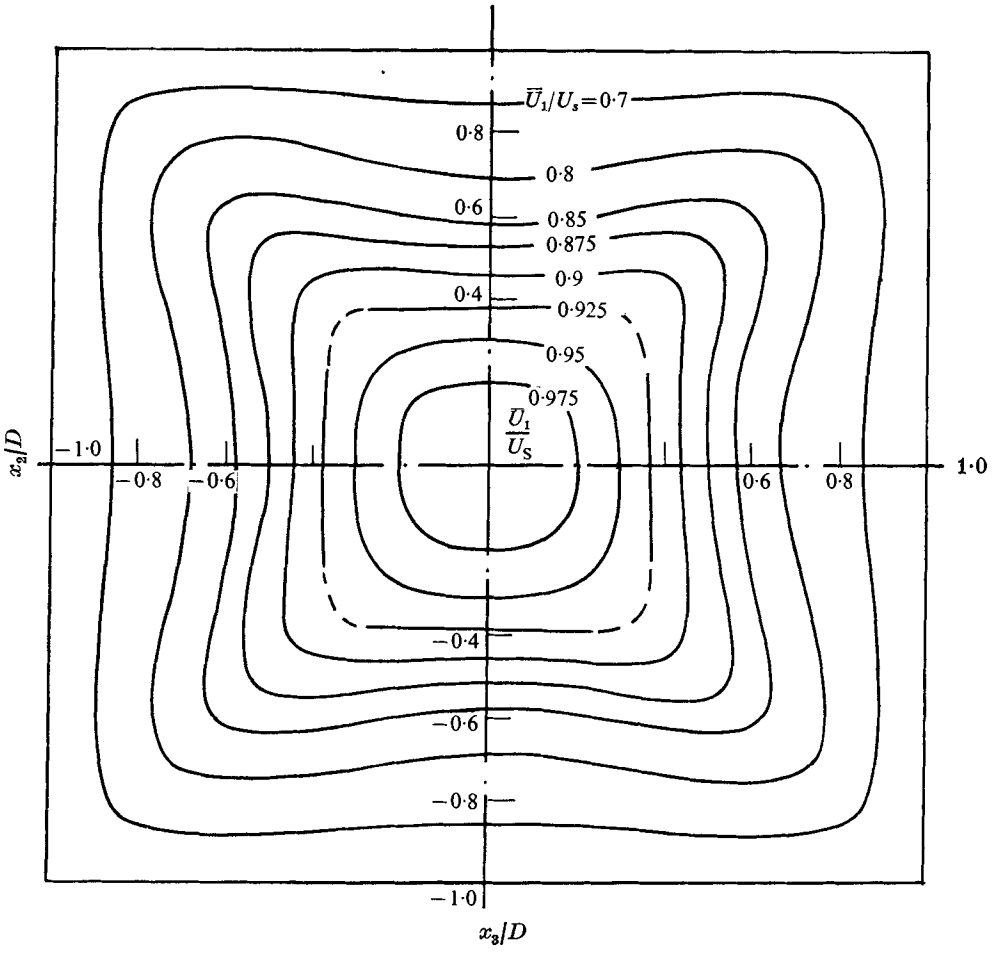

FIGURE 4. Mean velocity contours: $x_1/D_H = 36{\cdot}8$.

Symmetry of the mean flow

Figure 4 presents contours of axial mean velocity (isovels) at the station closest to the downstream end of the duct; it demonstrates the degree of symmetry which was achieved. The contour plots were drawn from mean velocity profiles measured across 13 horizontal planes spaced between the bottom and the top of the duct with 40 measurements per profile. Although the duct cross-section was not exactly square, the contours have been plotted on a square grid with the distances x_2 and x_3 normalized by D_y and D_z respectively (figure 2). The contour plots were constructed faithfully from the data; severe smoothing was unnecessary because the measurements were of high quality, as shown by representative profiles of mean and r.m.s. quantities reported by Melling (1975).

The isovels in figure 4 represent a great improvement over the earlier measurements of Melling & Whitelaw (1973), which showed that distortions of isovels near the duct inlet influenced the entire downstream flow. Details of the modifications needed to improve the symmetry are described by Melling (1975).

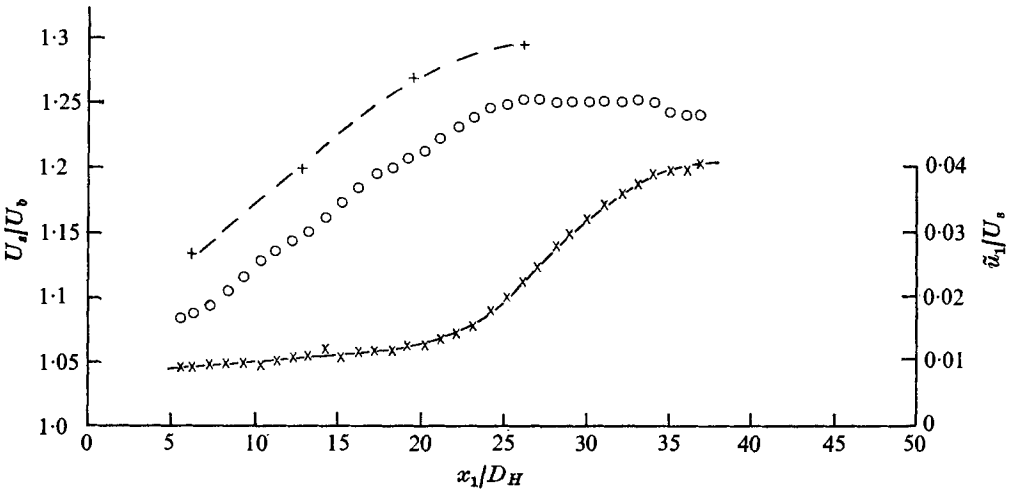

FIGURE 5. Variation of mean velocity and turbulence intensity along duct axis. +, U_s/U_b, Ahmed & Brundrett (1971), $Re = 8{\cdot}8 \times 10^4$; ○, U_s/U_b, present results, $Re = 4{\cdot}2 \times 10^4$; ×, $\tilde{u}_1/U_s$, present results.

The degree of symmetry of the isovels at $x_1/D_H = 36{\cdot}8$ is excellent; the maximum asymmetry in mean velocity profiles, with respect to the plane $x_2 = 0$, was about 1 % of U_s for $|x_2/D| < 0{\cdot}9$ and about 3·5 % for $|x_2/D| < 0{\cdot}95$. These figures are at least as good as those in other experiments reported in the literature. Ahmed & Brundrett (1971) reported symmetry of $\overline{U}_1$ to within 3 %, but they did not specify how close to the walls the symmetry was checked. Launder & Ying (1972) found that $\overline{U}_1$ was symmetric to within 1½ % along each of the axes $x_2 = 0$ and $x_3 = 0$, but this is an insensitive test; isovels in the same duct measured over the full cross-section by Thomas & Easter (1972) revealed that the overall asymmetry was very much worse. The most thorough check for symmetry was made by Gessner (1964), who measured the axial mean velocity, one component of the secondary velocity and all components of the Reynolds-stress tensor at several points in each quadrant; he obtained symmetry comparable with that in figure 4. In the present investigation, detailed mean and fluctuating velocity measurements were made in one quadrant only.

Axial variation of the mean flow

The axial development of the mean flow was investigated by measuring the centre-line mean velocity U_s as a function of x_1, and the axial pressure gradient dp/dx_1. Values of U_s from the laser-Doppler anemometer were normalized by the bulk velocity U_b to produce figure 5. The ratio U_s/U_b increased as far as $x_1/D_H = 25$ as a result of the boundary-layer growth on the walls constricting and accelerating the core fluid; it then became almost constant before decreasing gradually as a result of redistribution of momentum across the duct, assisted by the secondary flows. Eventually U_s/U_b must reach a constant value when the flow is fully developed, but this stage was not reached within the present duct length.

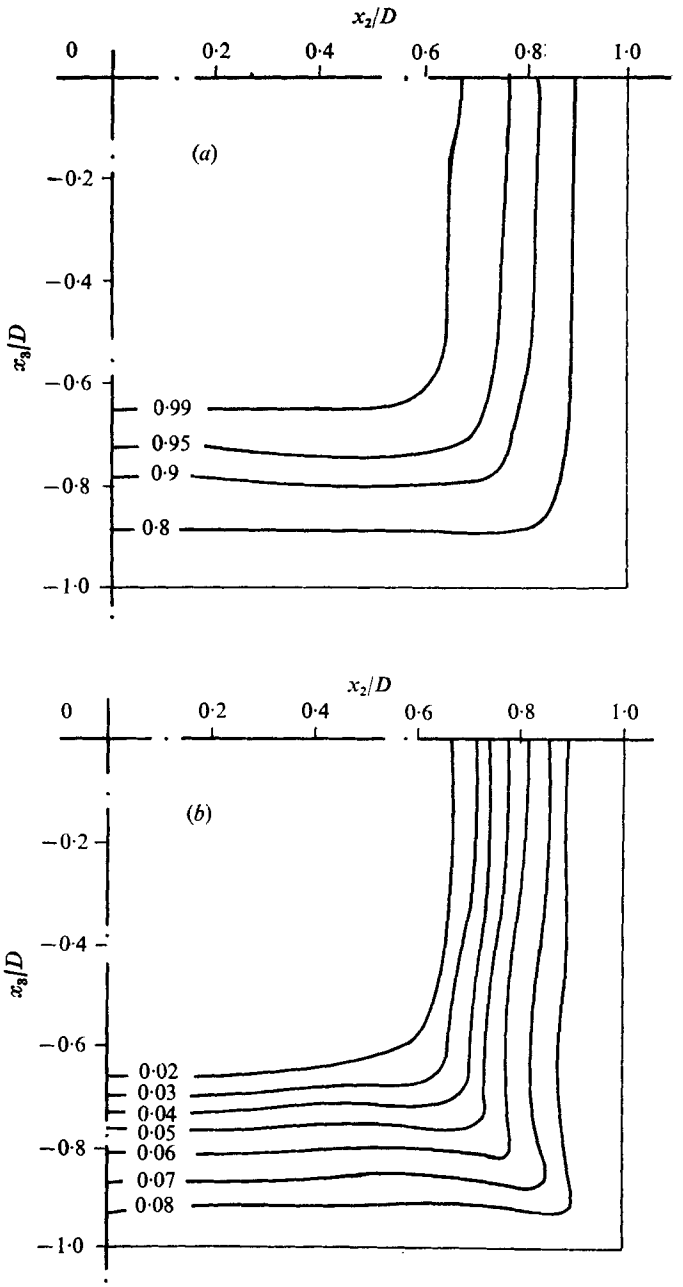

FIGURE 6. Contours of (*a*) $\bar{U}_1/U_s$ and (*b*) $\tilde{u}_1/U_s$: $x_1/D_H = 5{\cdot}6$.

The axial pressure gradient was linear within the scatter of the data throughout the region of flow development, although such behaviour would normally be expected only if the flow were fully developed. The average wall shear stress τ_w calculated from the pressure-gradient data using the equation

$$\tau_w = -\tfrac{1}{4}D_H\, dp/dx_1 \tag{3.1}$$

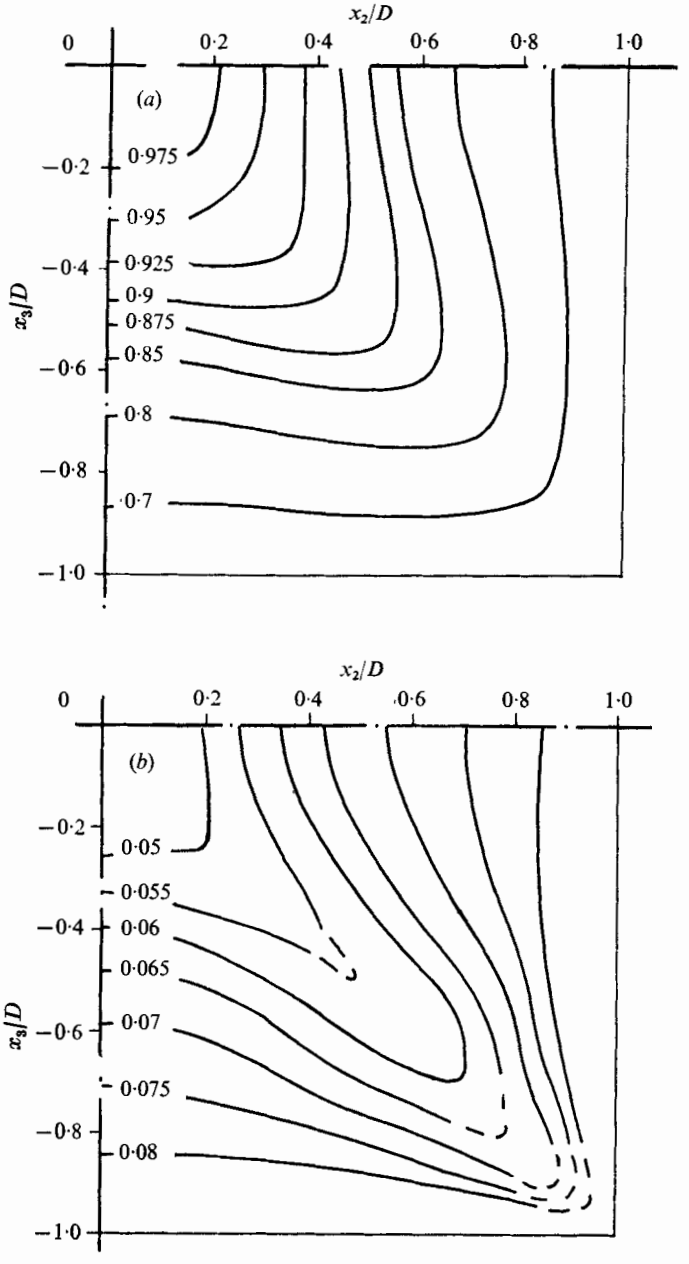

FIGURE 7. Contours of (*a*) $\bar{U}_1/U_s$ and (*b*) $\tilde{u}_1/U_s$: $x_1/D_H = 36{\cdot}8$.

was used to determine the friction velocity $U_\tau \equiv (\tau_w/\rho)^{\frac{1}{2}}$, where ρ is the fluid density. The friction velocity at a Reynolds number of $4{\cdot}2 \times 10^4$ was 0·049 m/s.

Axial mean velocity contours and profiles

Contours of axial mean velocity at five stations along the duct; i.e. x_1/D_H = 5·6, 13·2, 20·7, 29·0 and 36·8, were obtained and those at the first and last stations are shown on figures 6(*a*) and 7(*a*). The full set of contours showed that growth of the boundary layers and reduction in the central core of uniform velocity are accompanied by progressive deviation from two-dimensional flow, and bulging of the isovels towards the corner.

The velocity profiles were also plotted on Clauser charts to examine the extent to which they displayed a log-law profile typical of the inner region of two-dimensional boundary layers. The profiles at x_1/D_H = 36·8 showed that, except at $x_3/D = -0{\cdot}938$, where the influence of the corner was greatest, all the profiles conformed to a 'log-law' behaviour over a range of x_2. The values of $C_f \equiv \tau_w/\frac{1}{2}\rho U_s^2$ corresponding to each log-law region were unequal, indicating that the flow was not two-dimensional; but the peripheral distribution of τ_w could not be found from the C_f values at different x_3/D, since the error in determining τ_w was comparable with its small variation except near the corners. An average C_f gave $U_\tau = 0{\cdot}045 \pm 0{\cdot}001$ m/s; this value was 9 % smaller than that determined from pressure-gradient data. The profiles at upstream stations showed greater similarity over the log-law region, although at $x_1/D_H = 5{\cdot}6$ and 13·2 the sparseness of data within the thin boundary layers led to poor definition of the log-law region.

Axial turbulence intensity contours

Figures 6(*b*) and 7(*b*) show contours of the normalized axial turbulence intensity $\tilde{u}_1/U_s$. The highest r.m.s. levels plotted correspond to local intensities $\tilde{u}_1/\overline{U}_1$ of about 0·12. Higher r.m.s. levels were measured with the frequency tracker at positions closer to the walls, but observations of the tracker output suggested that these values were spuriously increased by drop-out. Corrections for gradient broadening, finite-transit-time broadening and instrument noise have been considered in detail (Melling 1975); but these were very small at almost all positions in the cross-sections at the five measuring stations, and were not included when plotting the contours of turbulence quantities. The turbulence intensity contours show a small asymmetry in the flow which was not revealed by the less sensitive mean velocity contours.

Compared with the corresponding isovels of $\overline{U}_1/U_s$, bulging of the contours towards the corners as a result of secondary velocities was more pronounced. The contours of $\tilde{u}_1/U_s$ bulged slightly towards the corner even at the first measuring station. At x_1/D_H = 20·7 the distortion was very strong, although it was still confined to a rather narrow region around the bisector where the isovels were curved; outside this region, both mean velocity and turbulence intensity contours were nearly parallel to the duct walls. At the next measuring station, x_1/D_H = 29·0, the distortion in the turbulence intensity contours had extended throughout the quadrant and a bulge had appeared in the isovels, suggesting the existence of an outward secondary flow near the diagonal.

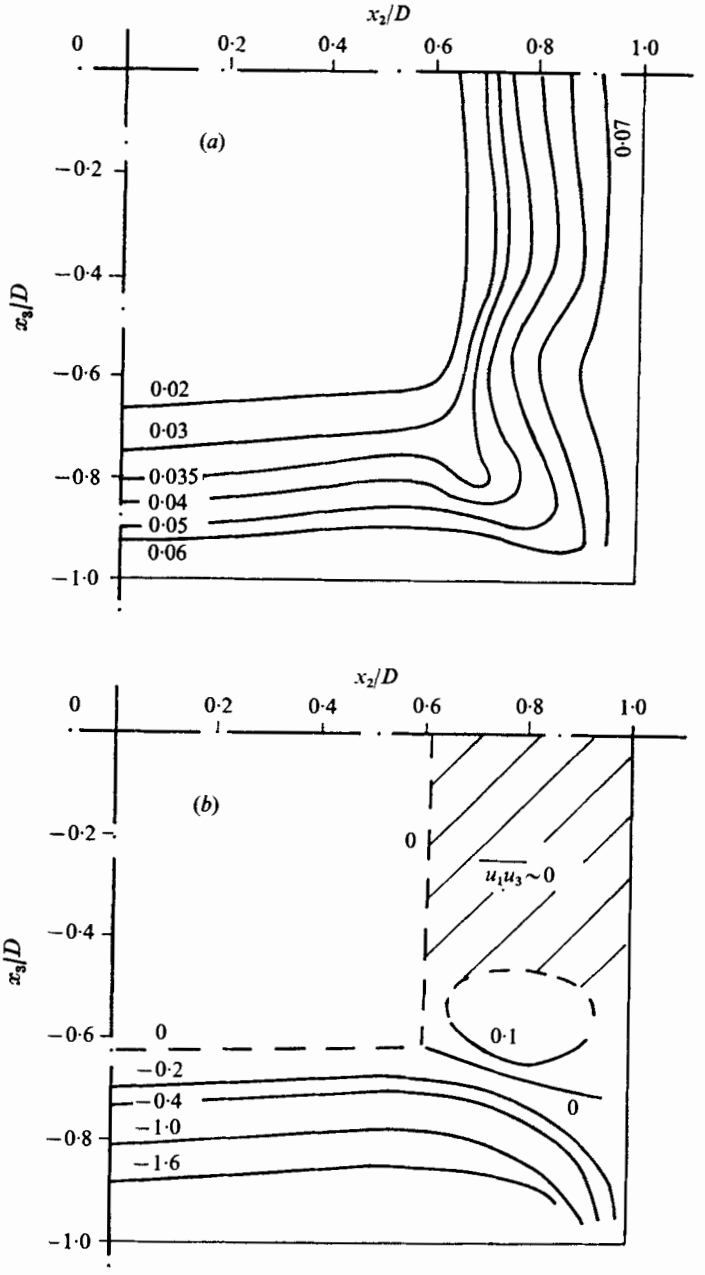

FIGURE 8. Contours of (a) $\tilde{u}_3/U_s$ and (b) $(\overline{u_1u_3}/U_s^2) \times 10^3$: $x_1/D_H = 5{\cdot}6$.

Figure 5 shows that the wall boundary layers met at the duct centre-line between these two stations, near $x_1/D_H = 22$, where there was a significant increase in the centre-line value of $\tilde{u}_1/U_s$ and a level region in the distribution of U_s/U_b. This figure shows that the flow had not reached a fully developed condition at $x_1/D_H = 36{\cdot}8$, since $\tilde{u}_1/U_s$ was still increasing slightly at the last measuring station.

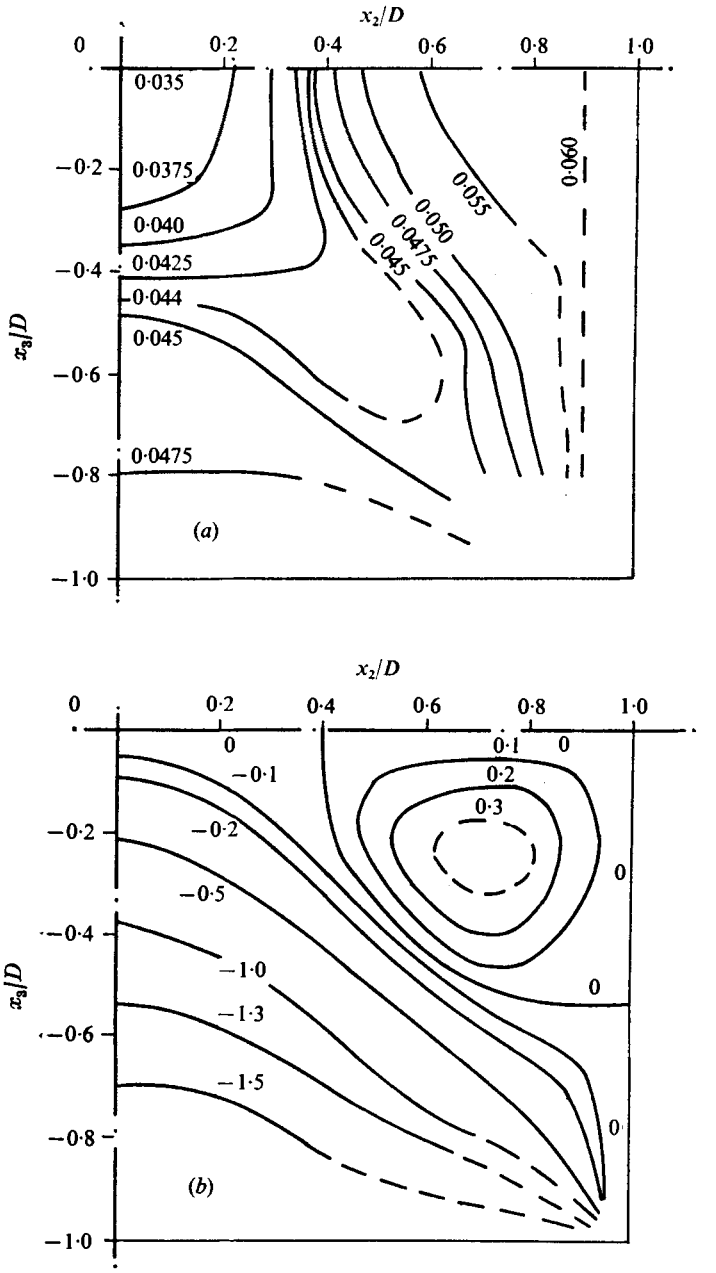

FIGURE 9. Contours of (*a*) $\tilde{u}_3/U_s$ and (*b*) $(\overline{u_1u_3}/U_s^2) \times 10^3$: $x_1/D_H = 36{\cdot}8$.

Transverse turbulence intensity contours

Contours of $\tilde{u}_3/U_s$ and $\overline{u_1u_3}/U_s^2$ at the stations $x_1/D_H = 5{\cdot}6$ and $36{\cdot}8$ are shown in figures 8 and 9 respectively; contours of $\tilde{u}_2/U_s$ and $\overline{u_1u_2}/U_s^2$ at $x_1/D_H = 36{\cdot}8$ are shown in figure 10. It would be unnecessary to measure $\tilde{u}_2$ and $\overline{u_1u_2}$ as well as $\tilde{u}_3$ and $\overline{u_1u_3}$ if the flow as a whole were symmetric. Consideri ng two points

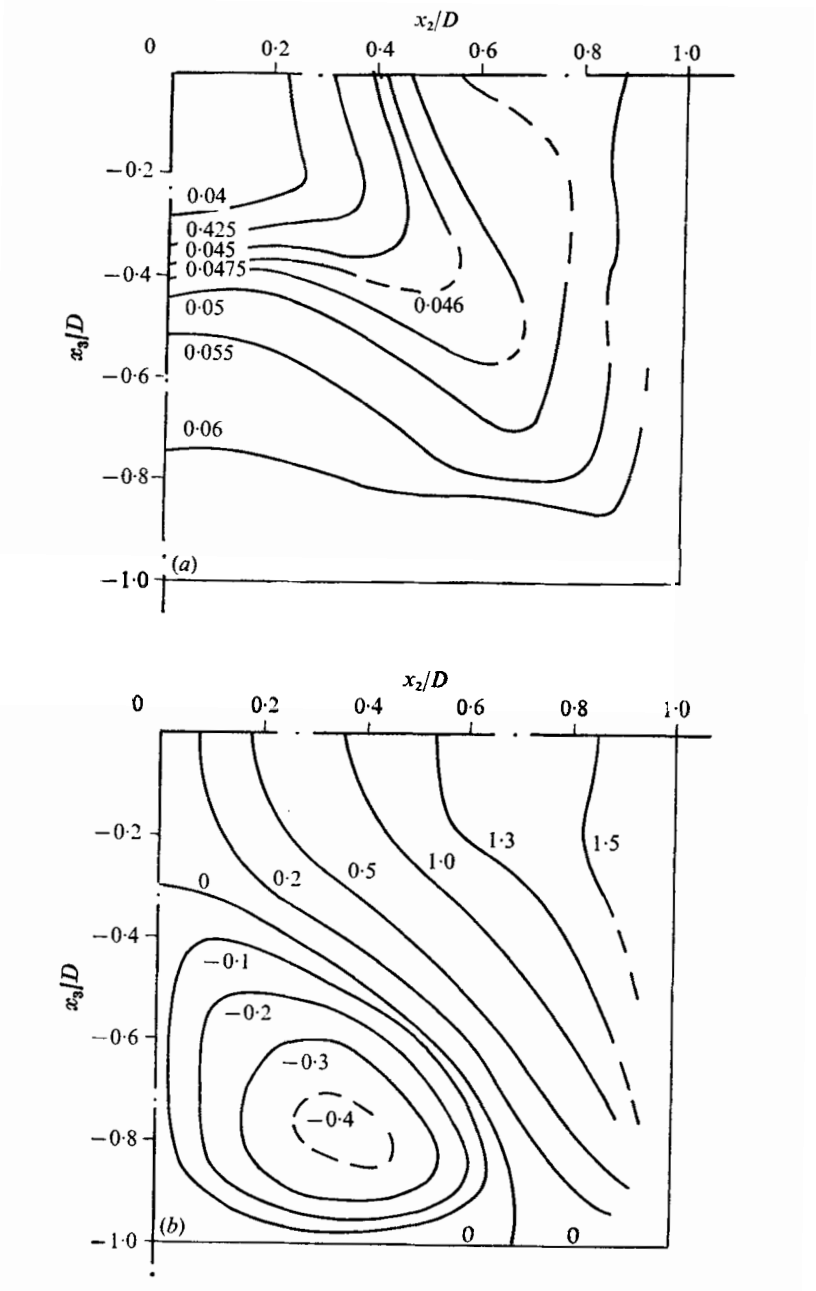

FIGURE 10. Contours of (*a*) $\tilde{u}_2/U_s$ and (*b*) $\overline{(u_1u_2}/U_s^2) \times 10^3$: $x_1/D_H = 36{\cdot}8$.

in the fourth quadrant of the duct symmetrically located with respect to the diagonal, i.e. $(x_1, x_B, -x_C)$ and $(x_1, x_C, -x_B)$, where $x_B \geqslant 0$ and $x_C \geqslant 0$, then overall symmetry of the flow requires

$$\tilde{u}_2(x_1, x_B, -x_C) = \tilde{u}_3(x_1, x_C, -x_B) \tag{3.2}$$

and

$$\overline{u_1u_2}(x_1, x_B, -x_C) = -\overline{u_1u_3}(x_1, x_C, -x_B). \tag{3.3}$$

In the present experiment, at $x_1/D_H = 36{\cdot}8$ symmetry of $\bar{U}_1$ about a diagonal was excellent, but asymmetry of $\tilde{u}_1$, while small, was noticeable. Thus $\tilde{u}_2$ and $\overline{u_1 u_2}$ were measured at $x_1/D_H = 36{\cdot}8$ to estimate the precision with which (3.2) and (3.3) were satisfied.

A notable feature of the distribution of $\tilde{u}_3/U_s$ at $x_1/D_H = 5{\cdot}6$ in figure 8(*a*) is the distortion of the contours over a much larger region of flow than for $\tilde{u}_1/U_s$ at the same station (figure 6*b*). The contours $\tilde{u}_1/U_s = 0{\cdot}02$ and $\tilde{u}_3/U_s = 0{\cdot}02$ lie at approximately the same position and may be considered to mark the edge of the boundary layer. Within the boundary layer $\tilde{u}_3$ increases more slowly towards the wall than $\tilde{u}_1$. This gradual variation is particularly pronounced in the contours of $\tilde{u}_3/U_s$ and $\tilde{u}_2/U_s$ at $x_1/D_H = 36{\cdot}8$ (figures 9*a* and 10*a*), where a change in $\tilde{u}_3/U_s$ as small as 0·001 would move a contour by about $0{\cdot}1D$ in the region near the diagonal. Equation (3.2) indicates that contours of $\tilde{u}_3/U_s$ and $\tilde{u}_2/U_s$ should be images of each other when reflected about a diagonal. Quantitative differences from this behaviour in figures 9(*a*) and 10(*a*) are attributable to the gradual variation of $\tilde{u}_2$ and $\tilde{u}_3$ across most of the cross-section, and to the sensitivity of the measurements to a small error in the inclination α of the fringe pattern.

Reynolds shear stress contours

Measurements of the shear stress $\overline{u_1 u_3}/U_s^2$ at $x_1/D_H = 5{\cdot}6$ were made difficult by the thinness of the boundary layers, and its distribution in figure 8(*b*) is not well defined in parts of the cross-section. $\overline{u_1 u_3}$ was zero over the region $|x_2/D| < 0{\cdot}6$, $|x_3/D| < 0{\cdot}6$, where the turbulence level was very low. For $x_3/D < -0{\cdot}6$, $\overline{u_1 u_3}/U_s^2$ increased towards the wall; except near the corner, the contours run roughly parallel to the wall, indicating that the boundary layer was approximately two-dimensional. In the region $x_2/D > 0{\cdot}6$, $x_3/D > -0{\cdot}6$ the shear stress was positive and very small but could not be determined with sufficient accuracy to draw contours; if the boundary layer were two-dimensional, $\overline{u_1 u_3}$ would be exactly zero throughout this region. $\overline{u_1 u_3}$ must be zero on the wall $x_2 = D$, and so the contours in the boundary layer on the wall $x_3 = -D$ turned towards the corner in order to satisfy the condition of zero wall shear stress. Near the wall, the shear stress should tend to a limit given by

$$-\overline{u_1 u_3}/U_s^2 = \tau_w/\rho U_s^2; \tag{3.4}$$

from measurements of τ_w, this limit was about $2{\cdot}4 \times 10^{-3}$, a value which is consistent with the results in figure 8(*b*).

The shear stress components $\overline{u_1 u_3}/U_s^2$ and $\overline{u_1 u_2}/U_s^2$ displayed a rather complicated behaviour at $x_1/D_H = 36{\cdot}8$, as shown in figures 9(*b*) and 10(*b*). The distribution of $\overline{u_1 u_3}$ was determined more reliably than at $x_1/D_H = 5{\cdot}6$, but evaluation of $\overline{u_1 u_3}$ was difficult in some parts of the cross-section, particularly for $x_2/D > 0{\cdot}9$, where small errors in the raw data led to a large scatter in profiles of $\overline{u_1 u_3}$. The contours of $\overline{u_1 u_3}/U_s^2$ in figure 9(*b*) can be related to the corresponding curves in figure 8(*b*). Since the boundary layers have grown to fill the entire duct cross-section the region of negative shear stress now occupies more than

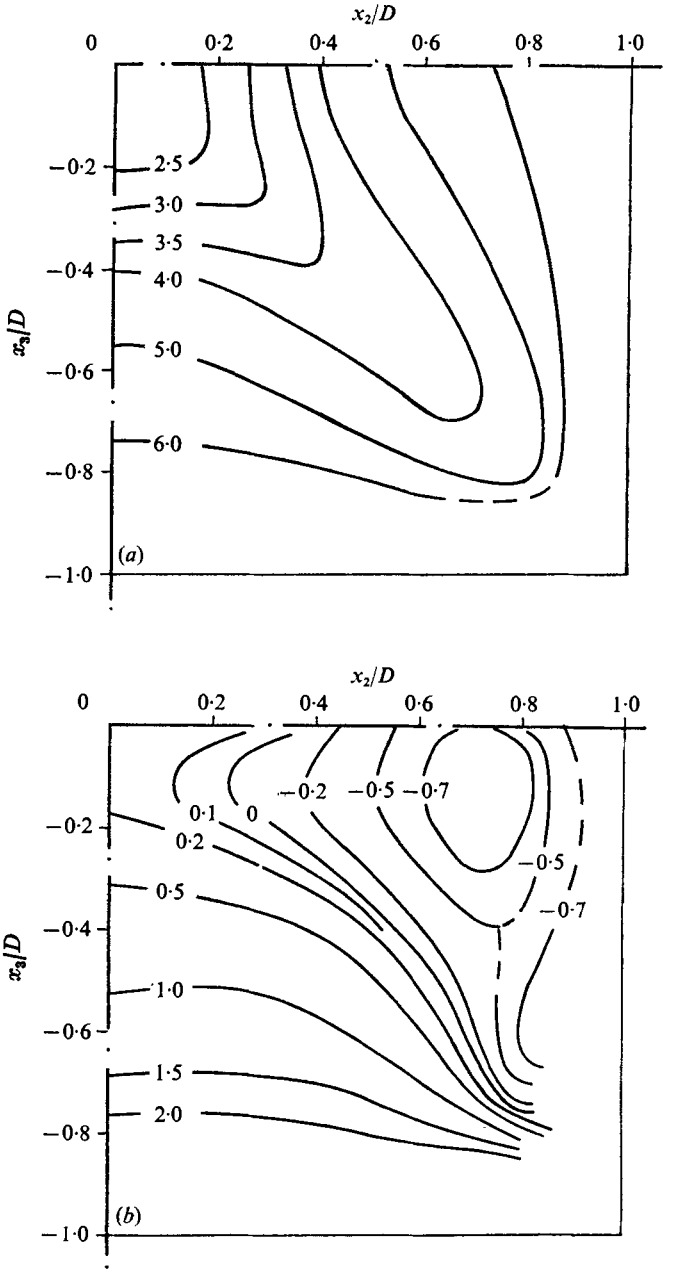

FIGURE 11. Contours of (*a*) $(k/U_s^2) \times 10^3$ and (*b*) $[(\overline{u_2^2} - \overline{u_3^2})/U_s^2] \times 10^3$: $x_1/D_H = 36{\cdot}8$.

half the quadrant, where the flow was no longer approximately two-dimensional. The contours bunch together towards the corner in order to satisfy the condition of zero shear stress on the wall $x_2 = D$, and magnitudes of $\overline{u_1 u_3}/U_s^2$ were compatible with the limiting wall value determined from (3.4). The closed contours of positive shear stress correspond to the region of near-zero shear stress in

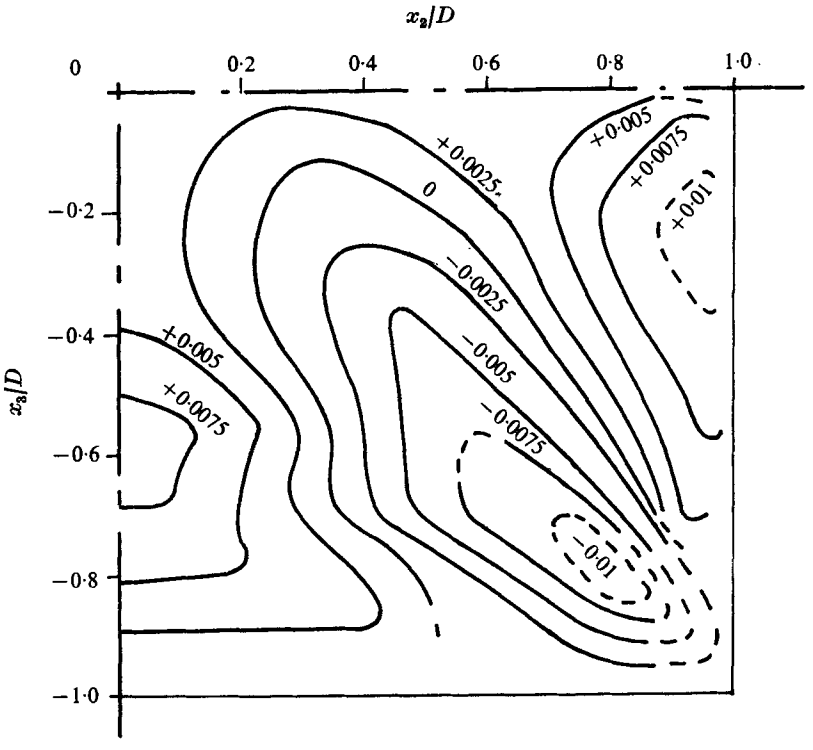

FIGURE 12. Contours of $\bar{U}_3/U_s$: $x_1/D_H = 36{\cdot}8$.

figure 8(*b*). They are bounded by the curve of zero shear stress, where profiles of $\overline{u_1 u_3}$ changed sign, and the conditions of zero shear stress on the wall $x_2 = D$ and on the x_2 axis. The maximum shear stress within this closed region was much smaller than that in the region of negative shear stress.

The features displayed by the contours of $\overline{u_1 u_2}$ in figure 10(*b*) are basically the same as for $\overline{u_1 u_3}$ except that the region of closed contours is larger. The relationship between $\overline{u_1 u_2}$ and $\overline{u_1 u_3}$ represented by (3.3), i.e. symmetry except for a change in sign after reflexion about a diagonal, is qualitatively satisfied by figures 9(*b*) and 10(*b*) but the quantitative agreement is less satisfactory. Since measurements were made in only one quadrant of the cross-section, it is possible that differences between the plots are indicative of asymmetry of the main flow; but it is more probable that the differences arise from uncertainties in measuring $\overline{u_1 u_2}$ and $\overline{u_1 u_3}$.

Kinetic energy contours

Figure 11 shows contours of the turbulent kinetic energy k/U_s^2 and the difference $(\overline{u_2^2} - \overline{u_3^2})/U_s^2$. If $\overline{u_1^2}$ is symmetrical about a diagonal, application of (3.2) indicates that k should also be symmetrical since $k \equiv \frac{1}{2}(\overline{u_1^2} + \overline{u_2^2} + \overline{u_3^2})$. The contours in figure 11(*a*) indicate fair symmetry, in spite of the differences between the

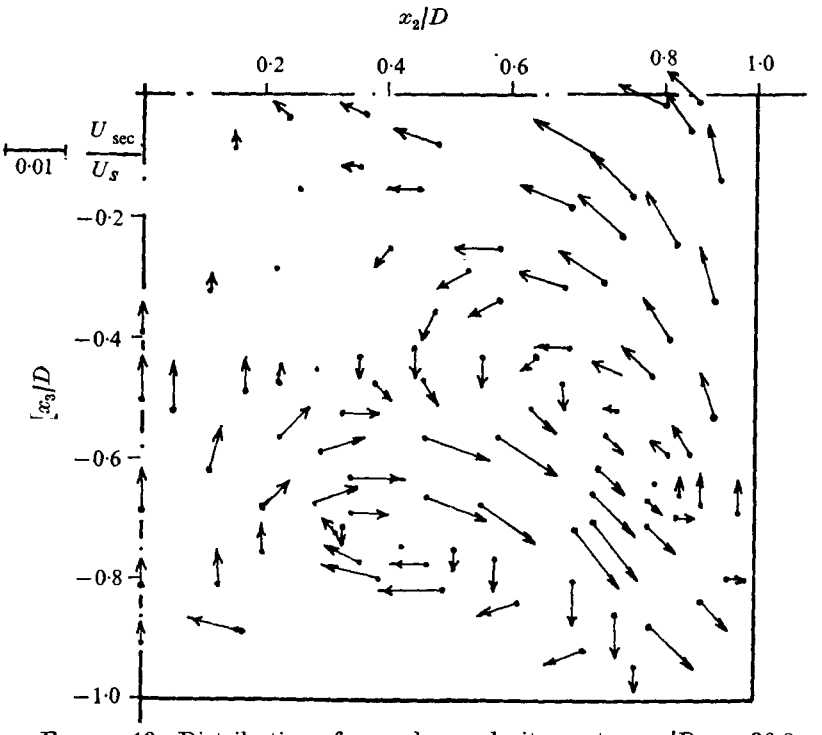

FIGURE 13. Distribution of secondary velocity vector: $x_1/D_H = 36{\cdot}8$.

contours of $\tilde{u}_3/U_s$ and $\tilde{u}_2/U_s$; the greatest deviation from symmetry is shown by the contour nearest to the wall.

The quantity $(\overline{u_2^2}-\overline{u_3^2})/U_s^2$ provides a very sensitive test of symmetry. If (3.2) is satisfied then

$$\overline{u_2^2}\,(x_1, x_B, -x_C)-\overline{u_3^2}\,(x_1, x_B, -x_C) = \overline{u_3^2}\,(x_1, x_C, -x_B)-\overline{u_3^2}\,(x_1, x_B, -x_C) \quad (3.5)$$

and contours of $(\overline{u_2^2}-\overline{u_3^2})/U_s^2$ should be antisymmetric about a diagonal. The contours in figure 11 (*b*) deviate from this condition and emphasize the differences between the measured contours of $\tilde{u}_2/U_s$ and $\tilde{u}_3/U_s$; they are thus very sensitive to experimental error. Contours in the region $x_2/D > 0{\cdot}8$ were very difficult to construct from the profile data, so the apparent local minimum centred near $x_2/D = 0{\cdot}7$, $x_3/D = -0{\cdot}15$ may not represent the actual flow.

Secondary mean velocity contours

Contours of the secondary velocity component $\overline{U}_3/U_s$ at $x_1/D_H = 36{\cdot}8$ are plotted in figure 12. The component $\overline{U}_2$ was also measured and combined with $\overline{U}_3$ to determine the magnitude

$$U_{\text{sec}} = (\overline{U}_2^2+\overline{U}_3^2)^{\frac{1}{2}} \quad (3.6)$$

of the secondary mean velocity and its direction

$$\theta_{\text{sec}} = \tan^{-1}(\overline{U}_3/\overline{U}_2) \quad (3.7)$$

relative to the x_2 axis. The distribution of the secondary velocity vector is plotted in figure 13, where the short horizontal bar represents a magnitude $U_{\text{sec}} = 0{\cdot}01\ U_s$. Maximum secondary velocities were little more than 1 % of U_s. The vectors indicate transport of fluid from the centre-line towards the corner, then from the corner towards the midpoints of the adjacent walls and finally back to the centre-line roughly parallel to the bisectors of the walls. This flow pattern accords with those reported by Hoagland (1960), Brundrett & Baines (1964), Gessner & Jones (1965) and Launder & Ying (1972).

In a symmetric flow, the secondary velocity components should be related in the fourth quadrant by

$$\overline{U}_2(x_1, x_B, -x_C) = -\overline{U}_3(x_1, x_C, -x_B), \tag{3.8}$$

with $\overline{U}_2 = 0$ on $x_2 = 0$ and $\overline{U}_3 = 0$ on $x_3 = 0$. Equation (3.8) requires that contours of $\overline{U}_2$ be the same as contours of $\overline{U}_3$ reflected in a diagonal except for a change of sign, a condition which the measured contours in figure 12 satisfied qualitatively. The vector distribution in figure 13 should be symmetric about the diagonal with each secondary vortex entirely contained within an octant of the cross-section; the most obvious deviation from this is the apparent secondary flow across the x_2 axis into the first quadrant of the cross-section. The discrepancies in these figures result from the measurements of $\overline{U}_2$ and $\overline{U}_3$ not satisfying the continuity equation; as will be discussed in §4, published measurements of secondary velocity obtained by the hot-wire technique are also deficient in this respect. In the present case, measurements of $\overline{U}_2$ and $\overline{U}_3$ were very sensitive to any uncertainty in the angle of orientation of the fringe pattern; an error in α of 0·3° would change $\overline{U}_3$ by 100 % or more at some points in the cross-section (appendix B).

4. Discussion of results

The main purpose of this section is to compare the present measurements with those reported in the literature. The discussion is presented in terms of the quantities referred to in the previous section and in the same sequence.

Axial variation of the mean flow

The axial development of the centre-line mean velocity shown in figure 5 is compared with measurements by Ahmed & Brundrett (1971). The initial increase in U_s/U_b found in the present results was more gradual than that reported by Ahmed & Brundrett, but their result is less reliable because the degree of symmetry achieved in their flow was inferior to that of the present flow and it is likely that the flow through the inlet to their duct was not a plug flow (Ahmed 1971, private communication to A. D. Gosman).

Axial mean velocity contours

The isovels of $\overline{U}_1/U_s$ in figures 6(*a*) and 7(*a*) indicate the flow development up to $x_1/D_H = 36{\cdot}8$. More complete results (Melling 1975) showed that as far as

$x_1/D_H = 20{\cdot}7$ the isovels were nearly parallel to the duct walls except near the diagonal, and the boundary layers on adjacent walls were developing almost independently. The first clear evidence of secondary flow in the isovels was found at $x_1/D_H = 29{\cdot}0$. Ahmed & Brundrett reported evidence of secondary flow at $x_1/D_H = 19{\cdot}6$, but this earlier influence is probably related to their more rapid increase in U_s shown in figure 5.

Comparison of the isovels measured at $x_1/D_H = 36{\cdot}8$ with those reported for fully developed flow by Brundrett & Baines (1964) indicates qualitative agreement although the latter tend to be flatter. Near the centre of the duct Launder & Ying's (1972) contours are close to those measured here, but near the wall they are closer to those of Brundrett & Baines. Launder & Ying's results may underestimate the distortion of the isovels since the velocity distribution, as reported by Thomas & Easter (1972), was substantially different from one quadrant to another.

Gessner's (1964) isovels for $Re = 1{\cdot}5 \times 10^5$ and $3{\cdot}0 \times 10^5$ indicate a more uniform distribution of velocity across the centre of the duct; for example, Gessner's isovel for $\overline{U}_1/U_s = 0{\cdot}8$ was almost coincident with that for $\overline{U}_1/U_s = 0{\cdot}7$ in the present results. The present distributions are more peaked than any reported previously, probably because of the shorter duct length ($36{\cdot}8D_H$, compared with $69D_H$ for Launder & Ying, $280D_H$ for Brundrett & Baines, and $40D_H$ with artificial boundary-layer thickening for Gessner).

Axial turbulence intensity contours

The only data on the axial turbulence intensity $\tilde{u}_1/U_s$ available for comparison with the present results are those of Brundrett & Baines (1964) and Gessner (1964) in fully developed flow. For $\tilde{u}_1/U_s \leqslant 0{\cdot}06$, agreement between the present contours and those of Brundrett & Baines is remarkably close. At higher turbulence intensities, agreement is reasonably close near the diagonal, but near the x_2 and x_3 axes the contours, particularly for $\tilde{u}_1/U_s = 0{\cdot}08$, are very different, perhaps because of the different stages of development of the flow in the two experiments.

In comparison with the present data and those of Brundrett & Baines near the centre of the duct, Gessner's data show less bulging along the diagonal and a more gradual increase in $\tilde{u}_1/U_s$. This behaviour is consistent with the more uniform mean velocity distribution which he found in this region of the flow. Closer to the wall, Gessner's contours tend towards those of Brundrett & Baines. Gessner indicated a reduction of $\tilde{u}_1/U_s$ approaching 20% when the Reynolds number was doubled from $1{\cdot}5 \times 10^5$ to $3{\cdot}0 \times 10^5$; if correct, this might account for the higher turbulence intensities near the centre in the present results, but would not explain the lower turbulence intensities near the wall.

Transverse turbulence intensity contours

Results for the transverse components of turbulence intensity, Reynolds shear stress and turbulence kinetic energy at $x_1/D_H = 36{\cdot}8$ can be compared with the fully developed flow measurements of Brundrett & Baines (1964) and Gessner

(1964). Brundrett & Baines's contours of $\tilde{u}_3/U_s$, constructed from their tabulated data, are in good agreement with the present $\tilde{u}_3/U_s$ results. Their results are preferable to the present ones near the walls and the corner, although their tabulated data contain some inconsistencies.

Gessner's contours of $\tilde{u}_3/U_s$, obtained from measurements of $\tilde{u}_2$ and $\tilde{u}_3$ in an octant of the duct, are broadly similar in shape to those in figure 9(*a*) although the position of maximum bulging was nearly on the diagonal. Comparison of magnitudes of $\tilde{u}_3/U_s$ is difficult because of the gradual variation across most of the duct, making location of contours very sensitive, but Gessner reported lower values across most of the duct cross-section, particularly near the duct centre. His results indicated an even greater reduction in $\tilde{u}_3/U_s$ than in $\tilde{u}_1/U_s$ when the Reynolds number was doubled.

Reynolds shear stress contours

For comparison with Brundrett & Baines's contours of $\overline{u_1 u_3}/U_\tau^2$, the contours from figure 9(*b*) were re-normalized using $U_\tau = 0{\cdot}045$ m/s. Qualitatively the two sets of contours are very similar; the region of positive shear stress found by Brundrett & Baines was more extensive than that for $\overline{u_1 u_3}$ in figure 9(*b*) but smaller than that for $\overline{u_1 u_2}$ in figure 10(*b*). A major difference lies in the magnitudes of $\overline{u_1 u_3}$ in the negative region. The present results indicate that $\overline{|u_1 u_3|}/U_\tau^2$ increases towards the wall, approaching the necessary boundary value of 1·0. Brundrett & Baines reported values of $\overline{|u_1 u_3|}/U_\tau^2$ in excess of 1·5 near the wall; this ratio could exceed 1·0 by a small amount because of the variation in τ_w along the wall, but their unduly high result may be caused by an erroneous normalization by $\frac{1}{2}U_\tau^2$ (Ahmed 1971, private communication to A. D. Gosman).

Gessner's contours of Reynolds shear stress do not conform to constraints imposed by the boundary conditions. In the octant bounded by the lines $x_2 = 0$, $x_3 = -D$ and $x_3 = -x_2$, contours were similar in shape to the present results, but $\overline{u_1 u_3}/U_\tau^2$ attained values of $-1{\cdot}50$ and $-1{\cdot}21$ near the bottom wall at $Re = 1{\cdot}5 \times 10^5$ and $3{\cdot}0 \times 10^5$ respectively. In the other octant the contours ran roughly parallel to the wall $x_2 = D$, incorrectly implying a finite shear stress on that wall. Gessner did not report a region of closed contours, although he did find one in a duct of aspect ratio 2:1.

Some further insight into the shape of the shear stress contours in figures 9(*b*) and 10(*b*) is obtained by modelling $\overline{u_1 u_2}$ and $\overline{u_1 u_3}$ by an effective viscosity; i.e.

$$-\overline{\rho u_1 u_2} = \mu_{\text{eff}}\, \partial \overline{U}_1/\partial x_2, \quad -\overline{\rho u_1 u_3} = \mu_{\text{eff}}\, \partial \overline{U}_1/\partial x_3,$$

in order to relate shear stress profiles to profiles of $\overline{U}_1$ deduced from figure 7(*a*). Along $x_3/D = -0{\cdot}2$, for example, $\partial \overline{U}_1/\partial x_2$ is negative everywhere and hence $\overline{u_1 u_2}$ is always positive and of increasing magnitude towards the wall at $x_2 = D$. Along $x_3/D = -0{\cdot}7$, however, $\partial \overline{U}_1/\partial x_2$ is zero on the x_3 axis and then becomes positive (because of the bulging of the isovels towards the corner), implying a negative turbulent shear stress. Near $x_2/D = 0{\cdot}6$, $\partial \overline{U}_1/\partial x_2$ becomes negative, leading to positive values of $\overline{u_1 u_2}$ as shown in figure 10(*b*). Similarly, by

considering the variation of $\partial\overline{U}_1/\partial x_3$ along lines of constant x_2, the features of $\overline{u_1 u_3}$ contours are explained. This model also reveals some discrepancies in the shear stress results. For example, from a traverse along $x_3/D = -0{\cdot}4$, the isovels in figure 7(*a*) do not show any region of positive $\partial\overline{U}_1/\partial x_2$ whereas figure 10(*b*) implies that $\partial\overline{U}_1/\partial x_2$ is positive for $x_2/D < 0{\cdot}25$; this suggests that the region of closed $\overline{u_1 u_2}$ contours is too large. Similarly, examination of $\partial\overline{U}_1/\partial x_3$ suggests that the region of closed contours in figure 9(*b*) is too small.

Kinetic energy contours

Contours of turbulence kinetic energy k/U_s^2 from figure 11(*a*) were normalized by U_τ^2 and compared with the measurements of Brundrett & Baines (1964) and the predictions of Launder & Ying (1973), based on a one-equation turbulence model. The measured and predicted contours all have approximately the same shape, although the levels of k/U_τ^2 are different. The kinetic energy level across the duct shown by the contours of the present experiment is lower than that reported by Brundrett & Baines; such a discrepancy is consistent with the possible error of normalization in their results. Differences between the present measurements and Launder & Ying's predictions are rather larger than those between the two sets of measurements, and are in the opposite direction. The exent of the discrepancy is not surprising in view of the simplicity of the turbulence model.

The contours of $(\overline{u_2^2}-\overline{u_3^2})/U_s^2$ shown in figure 11(*b*) do not satisfy the condition of antisymmetry with respect to the diagonal, and it was not possible to determine the extent to which the contours were affected by a real difference between $\overline{u_2^2}$ or $\overline{u_3^2}$ rather than a difference arising from measurement uncertainties. The measurement procedure adopted by Brundrett & Baines allowed them to determine $\overline{u_2^2}-\overline{u_3^2}$ more accurately than either $\overline{u_2^2}$ or $\overline{u_3^2}$, but the perfect antisymmetry shown by their contours was not necessarily representative of the actual flow since they were plotted from measurements in a triangular sector of the duct. It is unfortunate that $\overline{u_2^2}-\overline{u_3^2}$ is so difficult to measure since it is one of the most important quantities for generation of secondary motion, as shown by the equation for the mean flow vorticity, equation (3) of Brundrett & Barnes (1964).

Secondary mean velocity contours

A detailed comparison of the secondary mean velocity U_{sec} (figure 13) with the results for fully developed flow reported by Brundrett & Baines (1964), Gessner & Jones (1965) and Launder & Ying (1972) was not justified because of the uncertainty in all the results. In the measurements using laser-Doppler anemometry, error in determining the secondary velocity arose from the small difference between two comparatively large Doppler frequencies; the results were very sensitive to a small change in the orientation of the fringe pattern. This problem is likely to arise even if frequency-shifting is employed, with the fringe pattern arranged at $\alpha = 90°$ nominally. A small deviation from this alignment will cause the anemometer to detect a small part of the streamwise component of

velocity. Since this component is typically 100 times greater than the secondary velocity, measurement of the latter will be significantly in error. The hot-wire anemometer measurements were affected by uncertainty in determining the direction of the secondary velocity component, and by flow interference from the probe. An indication of the error in reported secondary velocity measurements can be found from the continuity equation. Gessner & Jones's secondary velocities showed a flow away from the wall about 20 % greater than that towards it, on all profiles. Launder & Ying found that the flows towards and from the wall agreed to within about 10 % at $x_2/D = 0{\cdot}2$ and $0{\cdot}5$, but at $x_2/D = 0{\cdot}8$ the flow away from the wall was five times as large as that towards it. The present measurements did not show a consistent trend; at $x_3/D = -0{\cdot}232$ the flow away from the wall was more than seven times that towards the wall, but at $x_3/D = -0{\cdot}794$ the flow away from the wall was only three-quarters of that towards the wall. Brundrett & Baines did not quantify any discrepancy between their results and the requirements of continuity, but their tabulated data do not fully satisfy the continuity equation. The symmetry of U_{sec} about a diagonal which they reported was a consequence of using measurements of $\overline{U}_2$ and $\overline{U}_3$ in an octant of the duct only; vectors of U_{sec} in the adjacent octant were then constructed from (3.8), assuming symmetry. The distribution of U_{sec} in figure 13 thus provides a realistic picture of the reliability with which secondary velocities can be measured.

5. Conclusions

Detailed measurements of the axial component of mean velocity and the corresponding normal stress have been made in the developing region of a rectangular duct flow. In the nearly fully developed region, the secondary components of the mean velocity and the corresponding normal and shear stresses were obtained. By using a laser-Doppler anemometer it was possible to take measurements in the region of flow development and thus to describe the flow more fully than is possible by hot-wire anemometry, where difficulties of probe access have restricted most of the results to fully developed flow.

The results confirm those qualitative features of turbulent flow through a rectangular duct previously indicated by the results obtained using hot-wire anemometry by Brundrett & Baines (1964) and Gessner & Jones (1965), but they indicate quantitative differences between the three sets of data. This disagreement emphasizes the difficulty of taking measurements in this flow configuration, whether by hot-wire or laser-Doppler anemometry, but the three sets of results together provide a better guide to the reliability of information than can be obtained from examination of a single set of data.

Measurements of the axial component of mean velocity and turbulence intensity in developing flow were an important part of the present study (Melling 1975) but space limitations prevented their inclusion in this paper. This work showed that the developing flow is much more sensitive to inlet conditions than a nominally fully developed flow, where it is usually considered that far enough from the duct inlet the results are independent of any peculiarities

of the rig. It is clear, however, that data on all components of mean velocity and Reynolds stress in the development region, combined with a precise specification of the flow at the inlet to the duct, would greatly assist the evaluation of prediction procedures for three-dimensional turbulent flows. The present results make a useful contribution to this requirement.

Measurements obtained in the nearly fully developed flow repeat those made by hot-wire anemometry. Contours of the Reynolds-stress components have not previously been presented in the form used in this paper, although data from which such contours may be derived were tabulated by Brundrett & Baines (1964). By taking measurements in a quadrant of the duct cross-section the stress components $\overline{u_2^2}$, $\overline{u_3^2}$, $\overline{u_1 u_2}$ and $\overline{u_1 u_3}$ were determined without the assumptions of symmetry implicit in previously published results where measurements were made in an octant only. The resulting contours also provide the fluid mechanicist with a better guide to the accuracy of Reynolds-stress data than hitherto. Frequency shifting was not used to obtain the results; it could be advantageous in the near-wall region, where the turbulence intensity reaches a maximum.

The laser-Doppler anemometer has an advantage over the hot-wire anemometer, particularly in measuring secondary velocity components, in that there is no probe interference in the flow. Owing to the sensitivity of the measurements to the angle of the interference fringes in space and the small magnitude of the secondary velocity relative to the axial velocity, the secondary flow results did not satisfy continuity exactly. The error in the present measurements is, however, quantifiable, unlike that arising from probe interference; consequently the laser-Doppler anemometer results can provide a measure of the confidence levels associated with secondary velocity measurements.

The quantity $\overline{u_2^2} - \overline{u_3^2}$ was obtained from measurements of the individual stresses $\overline{u_2^2}$ and $\overline{u_3^2}$, whose magnitudes are large relative to their difference. Simultaneous measurements of these two components would, however, determine $\overline{u_2^2} - \overline{u_3^2}$ more precisely; thus existing X-wire measurements of this quantity are probably more satisfactory than the present results.

It remains to determine the optimum turbulence model for the calculation of non-circular duct flows and it is hoped that the present measurements will assist in this optimization. Maximum generality is likely to be achieved with an approach such as that proposed by Launder *et al.* (1975), which requires the solution of equations for $\overline{U}_1$, $\overline{U}_2$, $\overline{U}_3$, $\overline{u_1^2}$, $\overline{u_2^2}$, $\overline{u_3^2}$, $\overline{u_1 u_2}$, $\overline{u_1 u_3}$, $\overline{u_2 u_3}$ and ϵ, although it is likely that the equation for the turbulence dissipation rate ϵ will have to be improved. This equation was developed on the basis of boundary-layer flows and, as was indicated by Pope & Whitelaw (1976), flows not of boundary-layer type, such as those experienced in the plane of the duct, reveal its inadequacies. The solution of ten equations in a Reynolds-stress model is a comparatively expensive endeavour and computing costs increase even further when equations for thermal energy properties are added. Thus it is desirable to ascertain whether a less complicated model can lead to solutions of suitable precision and generality. Further examination of Tatchell's (1975) approach using a three-

dimensional boundary-layer calculation procedure solving equations for $\overline{U}_1$, $\overline{U}_2$, $\overline{U}_3$, k and ϵ is desirable in the light of the present measurements and others which may be forthcoming for non-circular duct geometries.

The authors are glad to acknowledge financial support from the Central Electricity Generating Board and to record their thanks to Mr A. Hitchcock, Mr C. Lawn and Dr B. E. Launder for useful discussions at various stages of the experimental programme. Ms S. Chambers provided invaluable help with the preparation and typing of the manuscript.

Appendix A. Data reduction equations

For the horizontal-axis laser-Doppler anemometer sensitive to instantaneous velocities U_1 and U_3, the instantaneous output from the tracker is a voltage proportional to the Doppler frequencies ω_D, ω_D^+ and ω_D^- respectively for the three orientations of the fringe system. The Doppler frequencies measured in cases A, B and C respectively of figure 3(a) are

$$\omega_D = K\,U_1, \quad \omega_D^+ = K(U_1\cos\alpha + U_3\sin\alpha), \quad \omega_D^- = K(U_1\sin\alpha - U_3\cos\alpha), \tag{A 1)–(A 3}$$

where K is the proportionality constant between Doppler frequency and velocity, i.e. $K \equiv (4\pi\sin\phi)/\lambda$.

After time averaging, (A 1)–(A 3) retain the same form except that ω_D and U are replaced by $\overline{\omega}_D$ and $\overline{U}$ respectively. $\overline{U}_3$ is conveniently found by combining (A 2) and (A 3), i.e.

$$\overline{U}_3 = K^{-1}\,(\overline{\omega_D^+}\sin\alpha - \overline{\omega_D^-}\cos\alpha), \tag{A 4}$$

or

$$\overline{U}_3 = (\overline{\omega_D^+} - \overline{\omega_D^-})/2^{\frac{1}{2}}\,K \tag{A 5}$$

if $\alpha = 45°$. The mean-square differences are

$$\tilde{\omega}_D^2 \equiv \overline{(\omega - \overline{\omega}_D)^2} = K^2\,\overline{u_1^2}, \tag{A 6}$$

$$(\tilde{\omega}_D^+)^2 \equiv \overline{(\omega_D^+ - \overline{\omega_D^+})^2} = K^2\,(\overline{u_1^2}\cos^2\alpha + 2\overline{u_1 u_3}\sin\alpha\cos\alpha + \overline{u_3^2}\sin^2\alpha) \tag{A 7}$$

and

$$(\tilde{\omega}_D^-)^2 = \overline{(\omega_D^- - \overline{\omega_D^-})^2} = K^2\,(\overline{u_1^2}\sin^2\alpha - 2\,\overline{u_1 u_3}\sin\alpha\cos\alpha + \overline{u_3^2}\cos^2\alpha), \tag{A 8}$$

where $u_i \equiv U_i - \overline{U}_i$. The normal stress $\overline{u_1^2}$ is found directly from (A 6), and the stress $\overline{u_3^2}$ is found from a combination of all three equations, i.e.

$$\overline{u_3^2} = K^{-2}[(\tilde{\omega}_D^+)^2 + (\tilde{\omega}_D^-)^2 - \tilde{\omega}_D^2]. \tag{A 9}$$

$\overline{u_3^2}$ is independent of α provided that the fringes in cases B and C of figure 3 are mutually perpendicular. The difference between (A 7) and (A 8) is

$$(\tilde{\omega}_D^+)^2 - (\tilde{\omega}_D^-)^2 = K^2\,(\overline{u_1^2}\cos 2\alpha + 2\overline{u_1 u_3}\sin 2\alpha - \overline{u_3^2}\cos 2\alpha), \tag{A 10}$$

so that for $\alpha = 45°$ the turbulent shear stress is simply

$$\overline{u_1 u_3} = (2K^2)^{-1}\,[(\tilde{\omega}_D^+)^2 - (\tilde{\omega}_D^-)^2]. \tag{A 11}$$

For arbitrary α, $\overline{u_1 u_3}$ can be obtained by eliminating $\overline{u_3^2}$ between (A 7) and (A 8) and then substituting for $\overline{u_1^2}$ from (A 6); the result is

$$\overline{u_1 u_3} = (2K^2)^{-1} [(\tilde{\omega}_D^+)^2 \cot \alpha - (\tilde{\omega}_D^-)^2 \tan \alpha - 2\tilde{\omega}_D^2 \cot 2\alpha]. \quad \text{(A 12)}$$

Equations for $\overline{u_2^2}$ and $\overline{u_1 u_2}$ are derived in an analogous manner.

Appendix B. Errors in secondary velocity and Reynolds shear stresses

Systematic errors in $\overline{U}_2$, $\overline{U}_3$, $\overline{u_1 u_2}$ and $\overline{u_1 u_3}$ can arise from an error in the orientation angle α of the normal to the anemometer fringe pattern. These quantities were evaluated from successive measurements of Doppler frequency obtained with the normal orientated with respect to the x_1 axis at nominal angles of 0°, +45° and −45°. The construction of the optical unit ensured that the angles between the three directions were 45° to within an uncertainty of ±1′; but it was not possible to determine angles relative to the x_1 axis with the same confidence. With the horizontal-axis system the uncertainty in α was about ±0·3°; with the vertical-axis system the uncertainty was greater, i.e. ±0·5°, because of greater difficulty in alignment.

An analysis for the effect on $\overline{U}_3$ and $\overline{u_1 u_3}$ of a small deviation ϵ in the angle α from 45° shows that the resulting fractional changes in $\overline{U}_3$ and $\overline{u_1 u_3}$ are approximately

$$\Delta \overline{U}_3 / \overline{U}_3 \simeq \epsilon \, \overline{U}_1 / \overline{U}_3$$

and

$$\Delta \overline{u_1 u_3} / \overline{u_1 u_3} \simeq \epsilon \, (\overline{u_1^2} - \overline{u_3^2}) / \overline{u_1 u_3}.$$

These formulae indicate that a small error ϵ can introduce systematic errors in $\overline{U}_3$ and $\overline{u_1 u_3}$. At most places in the cross-section of the duct, $\overline{U}_3 / \overline{U}_1 \lesssim 0{\cdot}01$; hence an error of only 0·3° ($\epsilon = 0{\cdot}005$ rad) gives $\Delta \overline{U}_3 / \overline{U}_3 \simeq 0{\cdot}5$. This sensitivity emphasizes the experimental difficulties in measuring the secondary mean velocities. The uncertainty in $\overline{u_1 u_3}$ can be large in the vicinity of the zero-shear-stress contours in figures 9 (*b*) and 10 (*b*) and this may account for the difference between the locations of this contour in the $\overline{u_1 u_3}$ and $\overline{u_1 u_2}$ plots. The possible error in Reynolds shear stress is clearly smallest where $\overline{u_1 u_3}$ is large. For example, from figures 7 (*b*) and 9 at $x_2 = 0$, $x_3/D = -0{\cdot}7$, $\tilde{u}_1/U_s = 0{\cdot}075$, $\tilde{u}_3/U_s \simeq 0{\cdot}045$ and $\overline{u_1 u_3}/U_s^2 = -1{\cdot}5 \times 10^{-3}$, so for $\epsilon = 0{\cdot}3°$

$$\Delta \overline{u_1 u_3} / \overline{u_1 u_3} \simeq -2{\cdot}4\epsilon = -0{\cdot}012.$$

$\tilde{u}_3$ and $\tilde{u}_2$ are not affected by a systematic error in α, as noted in (A 9).

REFERENCES

AHMED, S. & BRUNDRETT, E. 1971 Turbulent flow in non-circular ducts. Mean flow properties in the developing region of a square duct. *Int. J. Heat Mass Transfer*, **14**, 365.

BRUNDRETT, E. & BAINES, W. D. 1964 The production and diffusion of vorticity in duct flow. *J. Fluid Mech.* **19**, 375.

DURÃO, D. F. G. & WHITELAW, J. H. 1974 Performance characteristics of two frequency-tracking demodulators and a counting system. *Proc. 2nd Int. Workshop on Laser Velocimetry, Purdue Univ.* vol. 1, p. 170.

DURST, F., MELLING, A. & WHITELAW, J. H. 1976 *Principles and Practice of Laser Doppler Anemometry*. Academic.

DURST, F. & ZARÉ, M. 1974 Removal of pedestals and directional ambiguity of optical anemometer signals. *Appl. Optics*, **13**, 2562.

GESSNER, F. B. 1964 Turbulence and mean-flow characteristics of fully-developed flow in rectangular channels. Ph.D. thesis, Purdue University.

GESSNER, F. B. 1973 The origin of secondary flow in turbulent flow along a corner. *J. Fluid Mech.* **58**, 1.

GESSNER, F. B. & JONES, J. B. 1965 On some aspects of fully-developed turbulent flow in rectangular channels. *J. Fluid Mech.* **23**, 689.

HARTNETT, J. P., KOH, J. C. Y. & MCCOMAS, S. T. 1962 A comparison of predicted and measured friction factors for turbulent flow through rectangular ducts. *Trans. A.S.M.E., J. Heat Transfer*, C **84**, 82.

HOAGLAND, L. C. 1960 Fully developed turbulent flow in straight rectangular ducts. Ph.D. thesis, MIT.

LAUNDER, B. E., REECE, G. J. & RODI, W. 1975 Progress in the development of a Reynolds-stress turbulence closure. *J. Fluid Mech.* **68**, 537.

LAUNDER, B. E. & YING, W. M. 1972 Secondary flows in ducts of square cross-section. *J. Fluid Mech.* **54**, 289.

LAUNDER, B. E. & YING, W. M. 1973 Prediction of flow and heat transfer in ducts of square cross-section. *Heat & Fluid Flow*, **3**, 115.

LEUTHEUSSER, H. J. 1963 Turbulent flow in rectangular ducts. *J. Hyd. Div., Proc. A.S.C.E.* **89** (3), 1.

MELLING, A. 1975 Investigation of flow in non-circular ducts and other configurations by laser Doppler anemometry. Ph.D. thesis, University of London.

MELLING, A. & WHITELAW, J. H. 1973 Measurements in turbulent water and two-phase flows by laser anemometry. *Proc. 3rd Bien. Symp. Turbulence in Liquids, Univ. Missouri, Rolla*, p. 115.

NAOT, D., SHAVIT, A. & WOLFSHTEIN, M. 1974 Numerical calculation of Reynolds stresses in a square duct with secondary flow. *Wärme- u. Stoffübertragung*, **7**, 151.

NIKURADSE, J. 1926 Untersuchungen über die Geschwindigkeitsverteilung in turbulenten Strömungen. *VDI-Forschungsheft*, p. 281.

PERKINS, H. J. 1970 The formation of streamwise vorticity in turbulent flow. *J. Fluid Mech.* **44**, 721.

POPE, S. B. & WHITELAW, J. H. 1976 The calculation of near-wake flows. *J. Fluid Mech.* **73**, 9.

TATCHELL, D. G. 1975 Convection processes in confined three-dimensional boundary layers. Ph.D. thesis, University of London.

THOMAS, D. L. & EASTER, P. G. 1972 Measurements of wall shear stress in a duct of square cross-section. *C.E.G.B. Rep.* RD/B/N2477.